Solar Phys (2013) 285:71–82
DOI 10.1007/s11207-012-0162-y

MESSENGER Observations of Magnetohydrodynamic Waves in the Solar Corona from Faraday Rotation

E.A. Jensen · M. Nolan · M.M. Bisi · I. Chashei · F. Vilas

Received: 26 March 2012 / Accepted: 8 October 2012 / Published online: 7 December 2012

Abstract During the declining phase of the longest solar minimum in a century, the arrival of the MESSENGER spacecraft at superior conjunction allowed the measurement of magnetohydrodynamic (MHD) waves in the solar corona with its 8 GHz radio frequency signal. MHD waves crossing the line of sight were measured via Faraday rotation fluctuations (FRFs) in the plane of polarization (PP) of MESSENGER's signal. FRFs in previous observations of the solar corona (at greater offset distances) consisted of a turbulent spectrum that decreased in power with increasing frequency and distance from the Sun. Occasionally a spectral line, a distinct peak in the power spectral density spectrum around 4 to 8 mHz,

Observations and Modelling of the Inner Heliosphere
Guest Editors: Mario M. Bisi, Richard A. Harrison, and Noé Lugaz

E.A. Jensen (✉) · F. Vilas
Planetary Science Institute, 1700 E. Ft. Lowell, Ste. 106, Tucson, AZ 85719-2395, USA
e-mail: ejensen@psi.edu

F. Vilas
e-mail: fvilas@psi.edu

E.A. Jensen
ACS Consulting/ACS Engineering & Safety, 40 Cypresscreek Pkwy, PMB 370, Houston, TX 77090, USA
e-mail: eaj@acs-consulting.com

M. Nolan
NAIC/Arecibo Observatory, HC-3 Box 53995, Arecibo, PR 00612, USA
e-mail: nolan@naic.edu

M.M. Bisi
Institute of Mathematics and Physics, Physical Sciences Building, Aberystwyth, Ceredigion SY23 3BZ, UK
e-mail: mario.bisi@aber.ac.uk

I. Chashei
Lebedev Institute of Physics, Pushchino Radio Astronomy Observatory, 142290 Pushchino, Russian Federation
e-mail: chashey@prao.ru

was also observed in these early data sets at offset distances of about 5 to 10 solar radii. The MESSENGER FRF data set shows a spectral line at an offset distance between 1.55 to 1.85 solar radii with a frequency of 0.6 ± 0.2 mHz. Other possible spectral lines may be at 1.2, 1.7, and 4.5 mHz; MHD waves with these same frequencies have been observed in X-ray data traveling along closed coronal loops at lower offset distances. An initial analysis of the MESSENGER spectral line(s) shows behavior similar to turbulent spectra: decreasing power with increasing frequency and distance from the Sun. Here we detail the steps taken to process the MESSENGER change in PP data set for the MHD wave investigation.

Keywords Solar cycle · Spacecraft · Magnetohydrodynamic waves · Solar corona · Radio frequency · Polarization · Faraday rotation · Faraday rotation fluctuations · Turbulence · Spectral lines · Alfvén waves · Magnetic field

1. Introduction

The solar wind drives Earth's space weather through a variety of mechanisms, including ram pressure when it interacts with the stationary geomagnetic field at supersonic, super-Alfvénic speeds and mixing (via reconnection) as a function of magnetic field strength and direction. The resulting geomagnetic storms can degrade communications, reduce spacecraft lifetimes, and have other significant negative effects including irradiating aircraft personnel. Understanding the generation and "evolution" of the solar wind with regard to its velocity, density, and magnetic field are critical in improving predictions of Earth's space weather.

The solar wind is generated in the solar corona, where it is heated and accelerated. Within the region of solar wind initiation between 1.05 and 15 solar radii, magnetohydrodynamic (MHD) waves play an important role in the transfer of energy and may act as the mechanism for coronal heating (Hollweg, 1986; Esser *et al.*, 1986). MHD modeling of coronal heating through the mechanism of turbulent heating has shown that periods of an hour (0.28 mHz) are capable of providing sufficient energy. While active regions (ARs) on the Sun radiating energy that can be observed with X-ray spectrometers have shown MHD waves propagating toward and away from the Sun (Van Doorsselaere, Birtill, and Evans, 2009), the majority of the Sun's magnetic field lines within the distances of interest (1.05 to 15 solar radii) are not visible through this technique. Only the phenomenon of Faraday rotation (FR) can measure the magnetic field within the region of solar wind generation outside of active regions (Bird, 1982).

A unique opportunity to investigate the mechanisms of solar wind generation occurred during the longest solar minimum in a century (the end of Solar Cycle 23). While Earth experienced few geomagnetic storms as a result of the minimum, the solar conditions generating the solar wind were sufficiently different that obtaining these observations provide an important measurement for temporal comparisons between solar cycles. In 2009, around the end of the minimum, the *MErcury Surface, Space ENvironment, GEochemistry, and Ranging* (MESSENGER) spacecraft entered superior conjunction, a situation that allowed the measurement of magnetohydrodynamic (MHD) waves in the solar corona using the Faraday rotation of MESSENGER's 8 GHz radio frequency signal (see Figure 4 in Jensen *et al.*, 2012, this issue). This Faraday rotation data set was taken in conjunction with a worldwide observing campaign of the heliosphere by the Interplanetary Scintillation (IPS) community (see, e.g., Hewish, Scott, and Wills, 1964; Armstrong and Coles, 1972; Bisi *et al.*, 2010; and references therein). During the observation period, the Pushchino Radio Astronomy Observatory showed that the heliosphere between 0.5 and 1 AU was in a quiet state.

Table 1 Wave types within the solar coronal plasma that affect Faraday rotation fluctuations.

Wave type	Magnetic field fluctuations	Electron density fluctuations
Hydrodynamic	No	Yes
Alfvén (MHD)	Yes	No
Magnetosonic (MHD)	Yes	Yes

2. Background

The analysis of MHD waves in the solar corona with Faraday rotation began with the observation of Faraday rotation fluctuations (FRFs) through multiple superior conjunctions of the *Helios* spacecraft (Hollweg *et al.*, 1982). FRFs can be generated through several mechanisms (Table 1), including magnetic field variations alone (Alfvénic), hydrodynamic effects (no magnetic field fluctuation), or magnetosonic effects (both magnetic field and hydrodynamic fluctuations). Hollweg *et al.* analyzed the magnitude of the *Helios* FRFs to determine the strength of the background magnetic field required if the fluctuations were purely hydrodynamic, using the group velocity of the signal to measure the total electron content fluctuations. The magnetic field solution was then compared to the extrapolated magnetic field from the *Helios* spacecraft (within 1 AU) and showed that 96 % of the fluctuations in the Faraday rotation observations were due to the fluctuations in the magnetic field. This result indicated that the observed FRFs (between 2 and 15 solar radii) were dominated by Alfvén waves.

The Alfvén waves observed in FRFs are undetectable beyond 15 solar radii; however, *in situ* Alfvénic fluctuations have been measured by magnetometers on spacecraft from the minimum perigee of the *Helios* spacecraft (60 Rs) out to Earth orbit (Belcher and Davis, 1971). Chashei *et al.* (1999) periodically observed a spectral line within the *Helios* FRF spectra at about 3.5 mHz (4.8 min) at offsets of around four solar radii. Taken at offsets between 1.55 and 3.22 solar radii, closer to the Sun than any previous FRF experiment, the MESSENGER data set contains a clear spectral line at 0.6 mHz. This paper focuses on the measurement of FRF spectral lines and an initial comparison to turbulent FRF observations.

2.1. Faraday Rotation

Faraday rotation, the rotation in the plane of polarization (PP) of an electromagnetic (EM) wave as it traverses a circularly birefringent medium, is the line-of-sight integral of the component of the magnetic field parallel to the line of sight weighted by the electron density when observed in the solar corona:

$$FR = \frac{A}{f^2}\int_{SC}^{\oplus} N\mathbf{B}\cdot \mathrm{d}\mathbf{s} \quad \text{[radians]},$$
$$A = \frac{q^3}{8\pi^2\epsilon_o m_e^2 c} = 2.3648\times 10^4 \quad \left[\frac{\mathrm{m^2\,rad}}{\mathrm{s^2\,T}}\right]. \tag{1}$$

The frequency of the signal (f) is in hertz, SC is the spacecraft, $\oplus$ is Earth, N is the electron density in [m^{-3}], s is the path of the signal in [m], q is the electron charge in [C], m_e is the mass of an electron in [kg], and c is the speed of light in a vacuum in [$\mathrm{m\,s}^{-1}$]. A positive FR means that the signal is rotated in a right-handed sense about the wave vector, the direction of travel of the electromagnetic wave.

In measuring Faraday rotation, one uses the calibrated change in the PP, where the PP is measured from the phase of the right and left circularly polarized components of MESSENGER's radio frequency signal:

$$PP = \frac{\phi_{\rm rcp} + \phi_{\rm lcp}}{2} \quad \text{[radians]}, \qquad FR = [M]PP \quad \text{[radians]}. \tag{2}$$

Here ϕ is the phase angle of the right and left circularly polarized waves (rcp and lcp), PP is the plane of polarization, and $[M]$ is the Mueller matrix used to calibrate the PP measurement to give the Faraday rotation FR; note that the effects of $[M]$ are slow varying over a period of hours and do not exceed 180°. *For PP rotations with higher frequency and over a range greater than* 180°, $\Delta PP \cong \Delta FR$. As we will discuss below, the change in the uncalibrated PP is approximately the same as the change in the Faraday rotation through a limited range of wave frequencies. This paper is focused on measuring the FRFs manifested in the change in the PP observations.

The signal from the MESSENGER spacecraft (8 GHz carrier frequency) traveled from the opposite side of the Sun to Earth through the solar plasma. Figures 2 and 3 in Jensen *et al.* (2012, this issue) illustrate the modeled Faraday rotation expected during ingress (8 November 2009) and egress (10 November 2009) of the MESSENGER superior conjunction time period. The measurement of Faraday rotation begins with observing the PP of the radio frequency signal. Whereas the information on the total amount of rotation requires continuous observation from large solar offsets (or multiple frequencies emitted by the source), the change in the Faraday rotation is the same as the change in the calibrated PP with time.

2.2. MHD Waves in Faraday Rotation

The plane of polarization (PP) measured at Earth changes when the plasma along the line of sight changes. For example, as shown in Figure 1, when an Alfvén wave crosses the line of sight, the component of the fluctuation along the line of sight introduces a similar fluctuation in the PP. If the line of sight is along the direction of the fluctuations (shown in Figure 1 as the y-direction), an Alfvén wave traversing in an orthogonal direction causes the PP to fluctuate with the changing component of the magnetic field along the line of sight. Because the component of the steady-state magnetic field is perpendicular to the line of sight in this orientation, the average Faraday rotation is zero (Figure 1, right panel). In contrast, if the line of sight is along the z-axis, parallel to the steady-state magnetic field, no fluctuation occurs in the 150° Faraday rotation (in this example), because the magnetic field fluctuations are perpendicular to the line of sight (Figure 1, top). Jensen and Russell (2009) discussed this point in further detail.

3. MESSENGER Plane-of-Polarization Measurements

The change in the PP in the MESSENGER data set is shown in Figure 2 (Jensen *et al.*, 2012). During each time period, the PP fluctuated about a mean slope. For the PP measurements on 8 November (blue), the size of the error bars through much of the time period were undetermined (red = determined, green = unknown); consequently, the steady-state background rotation could not be unwrapped. The 10 November time series was unwrapped as it rotated throughout the observation time period, and there was negligible steady-state background rotation on the 11 November time series.

System calibration errors occur over timescales of several hours and over the range of the expected parallactic rotation. The parallactic rotation is the expected apparent rotation

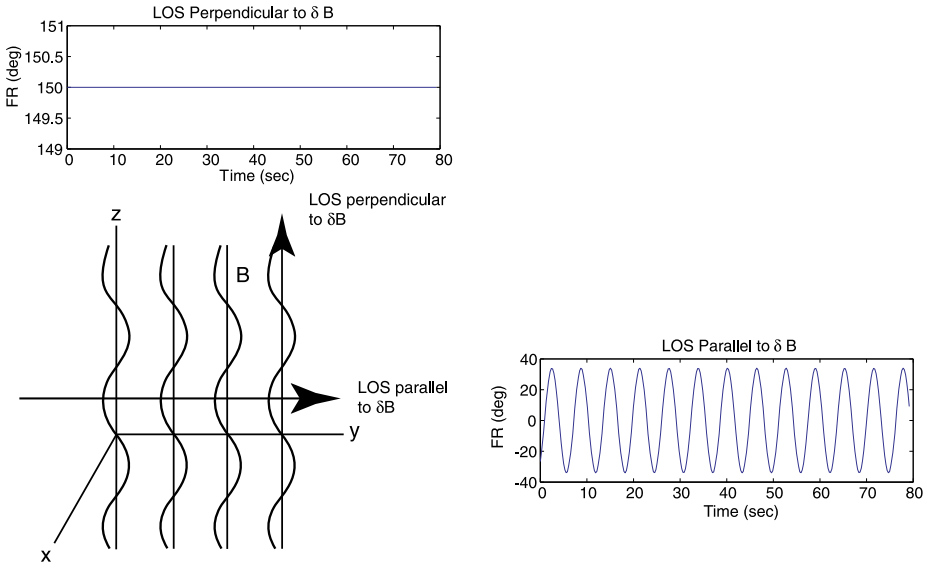

Figure 1 Effects of observer orientation on the observation of MHD wave propagation by Faraday rotation. FRFs are shown from two extremes in orientation: parallel and perpendicular to the direction of magnetic field fluctuations in an Alfvén wave propagating along the magnetic field line (shown here as the z-direction). The line of sight is perpendicular to the magnetic field fluctuations for the panel on top, and parallel to the fluctuations for the panel on the right (Jensen and Russell, 2009).

of a fixed polarization source as it is observed from a rotating reference frame (*i.e.*, Earth). Figure 3 shows the expected parallactic rotation during the MESSENGER experiment at the *Green Bank Telescope* (GBT), West Virginia. Over the 5.5 hours on 10 November from 12:00 UT to 17:30 UT, the expected rotation is positive 55°; this observing system rotation is markedly less than the rotation imposed by the solar corona. Approximately 10° of positive rotation is expected on 11 November over the 1.5 hours from 13:00 UT to 14:30 UT; this angle is visible in the data set. Finally, the expected rotation on 8 November is 60° over the 4.5 hours from 14:30 UT to 19:00 UT.

Jensen *et al.* (2012, this issue) reporting on the processing of the MESSENGER data set, shows that the coronal structural contribution to the Faraday rotation varies over a period of several hours, similar to the timescale for the parallactic rotation. Therefore, subtracting out the slowly varying background from the MESSENGER data set yields FRFs of solar origin with frequencies between 0.5 mHz and 5 mHz. Note that at MESSENGER's radio frequency of 8 GHz, the electron density of the Earth's ionosphere contributes almost no Faraday rotation to the observations. However, the Earth's ionosphere could play a significant role for Faraday rotation observations made using the new-generation radio telescope systems such as the *LOw Frequency ARray* (LOFAR) (Bisi *et al.*, 2011) based across Europe and the *Murchison Widefield Array* (MWA) based in Western Australia (*e.g.,* Salah *et al.*, 2005).

4. Removing Background Plane of Polarization

The identification of spectral lines occurs in two steps; these are summarized here and discussed further below. First, the best fit to the background slope is obtained using a highpass

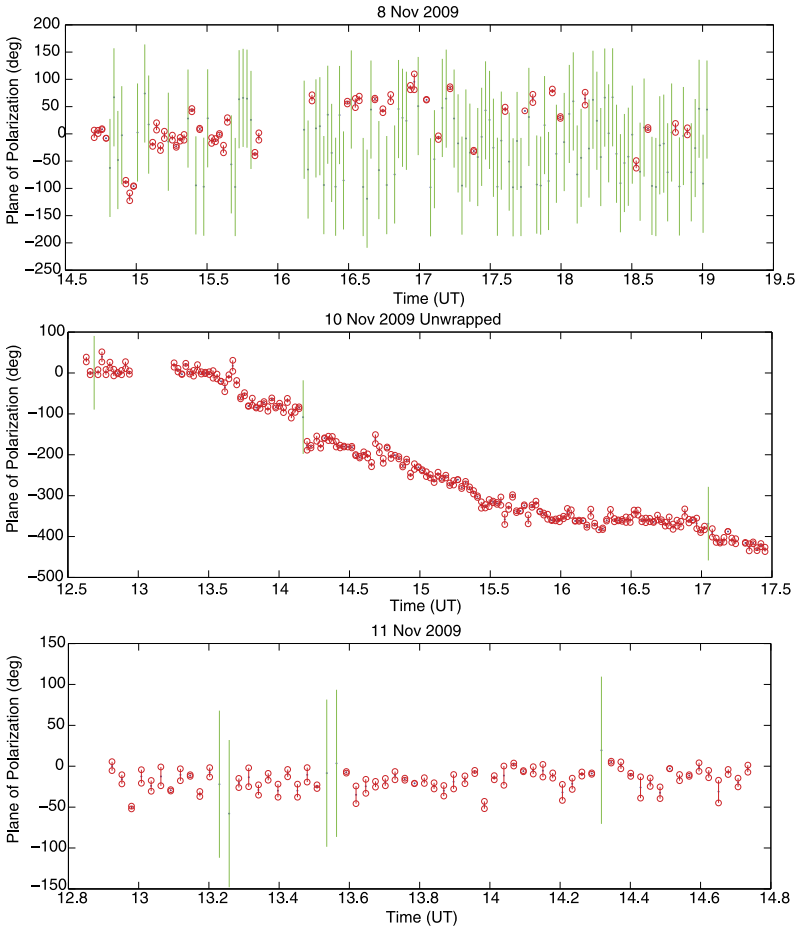

Figure 2 Change in the PP (blue) on 8 November (top), 10 November (middle), and 11 November (bottom) 2009, along with known error bars (red) and unknown error bars (green). The change in the PP on 10 November is strongly negative as predicted by the Faraday rotation model. The PP on 11 November has a negligible average slope, similar to the prediction. There are not enough 8 November observations to unwrap the change in the PP (Jensen *et al.*, 2012).

filter. Figures 4 and 5 (left) show the component of the data set that is removed by high-pass filtering. The spectrum from the filtered data set exhibits potential spectral lines whose ranges are defined as ± 0.2 mHz. The original data set has known error bars for each PP measurement. The reliability of the potential spectral line is measured by creating 1000 similar data sets within these error bars and measuring how consistently the spectral line occurs (Figures 6 and 7). Only the spectral line at 0.6 ± 0.2 mHz showed a good reliability (greater than two standard deviations).

By means of a method similar to that of Sakurai and Spangler (1994), the 10 and 11 November Faraday rotation data sets shown in Figure 2 were highpass filtered to remove the slowly varying background heliospheric field and system error contributions. Any data collected prior to a data gap were eliminated from the analysis.

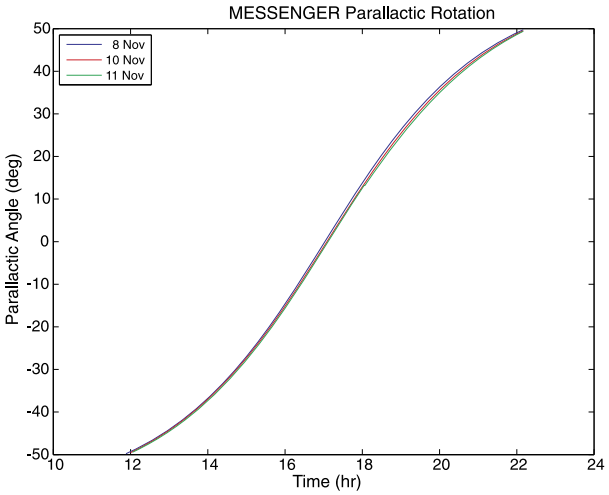

Figure 3 The parallactic angle at *Green Bank Telescope* (GBT). The change in the PP is caused by the noninertial coordinate system of the GBT antenna on the rotating Earth observing a fixed source in the sky.

Figure 4 (left) illustrates the method used to determine the ideal bandpass for 10 November 2009. The 0.125 and 0.25 mHz bandpasses were unable to fully block the slowly varying trend in the plane of polarization data: they taper off at the end. The 0.5 mHz and higher bandpasses were able to block the full trend. Note that the bandpass method used a Butterworth filter; this filter has an equal response across frequencies and *gradually* tapers off outside the bandpass. As shown in Figure 4 (right), the 0.6 mHz *potential* spectral line (pending further testing) persists even though the highpass filter had been set at 1 mHz. As expected with the tapering falloff in response outside the bandpass, the magnitude of the 0.6 mHz line is less; however, its continued presence indicates that it should be studied further.

Figure 5 (left) demonstrated that the highpass method for fitting the slowly varying trend in the PP on 11 November 2009 was not nearly as good as the linear fit. Note that whether the fit was linear or highpassed at 0.25, 0.5, and 1 mHz, the *potential* spectral line at 1.17 mHz persisted.

As shown, the other potential FRF spectral lines were unaffected by the frequency of the bandpass. However, these frequency ranges of interest in the FRF spectra must pass a reliability test in order to be considered a real spectral line. Note that the power spectral density (PSD) spectra were smoothed using Welch's method (Welch, 1967).

The reliability of the FRF spectral lines in the spectra for 10 and 11 November was determined using the PP error bars. Monte Carlo simulations created 1000 valid time series within the PP errors bars for each spectra. The PSD was calculated for each time series (Figures 6A and 7A), and the frequency of any lines within the bandpass was measured. The line frequencies were analyzed for the percentage that remained within ± 0.2 mHz of the data set line frequency. This percentage provided a measure of the reliability of the spectral line.

Results of the reliability analysis are given in Table 2. Figures 6B – F and 7B – D show the histograms of the distribution in the Monte Carlo spectra for the range of apparent spectral lines on 10 and 11 November. For example, the counts from the Monte Carlo spectra (Figure 6B) produced a central-frequency spectral line within ± 0.2 mHz frequency for 99.6 % of the 1000 runs. Similarly, the second, third, fourth, and fifth solutions (Figure 6C – F) had a central-frequency spectral line for 94.2 %, 44.8 % (clearly not a line), 61.9 %, and 74.7 % of the runs. The frequency range around 2.93 mHz with no Gaussian-like distribution is clearly not a spectral line;

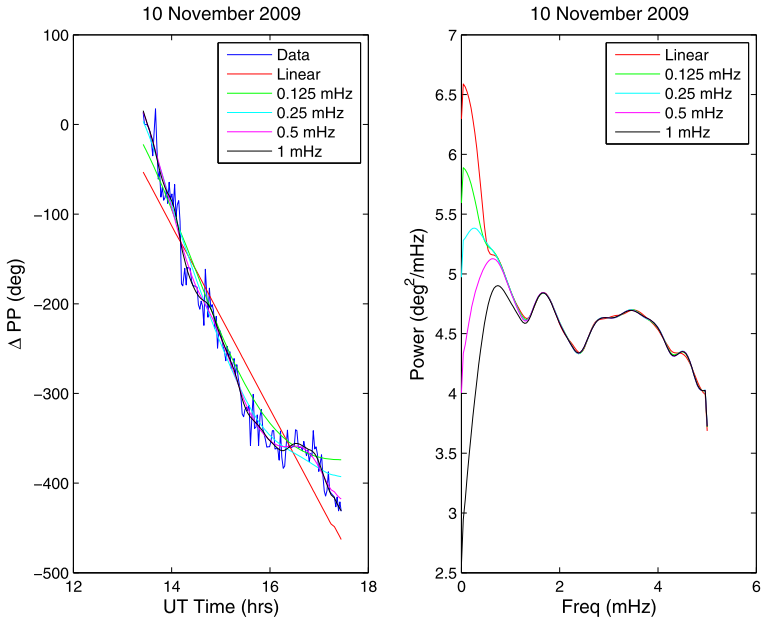

Figure 4 Fitting the background change in PP for removing it. The plot on the left shows the change in the PP on 10 November along with highpass fits plotted for varying bandpasses. The plot on the right shows the PSD spectrum of the residual FRFs from the different bandpasses.

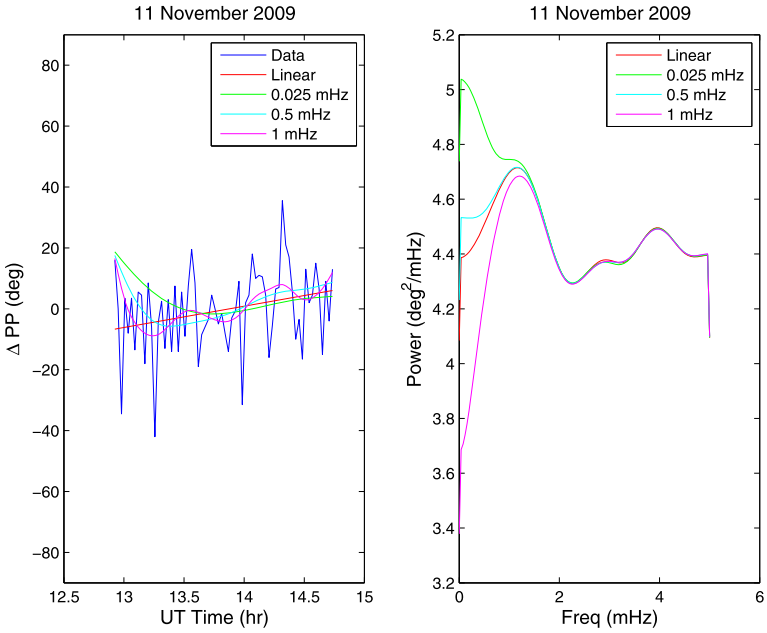

Figure 5 Fitting the background change in PP for removing it. The plot on the left shows the change in the PP on 11 November along with highpass fits plotted for varying bandpasses. The plot on the right shows the PSD spectrum of the residual FRFs from the different bandpasses.

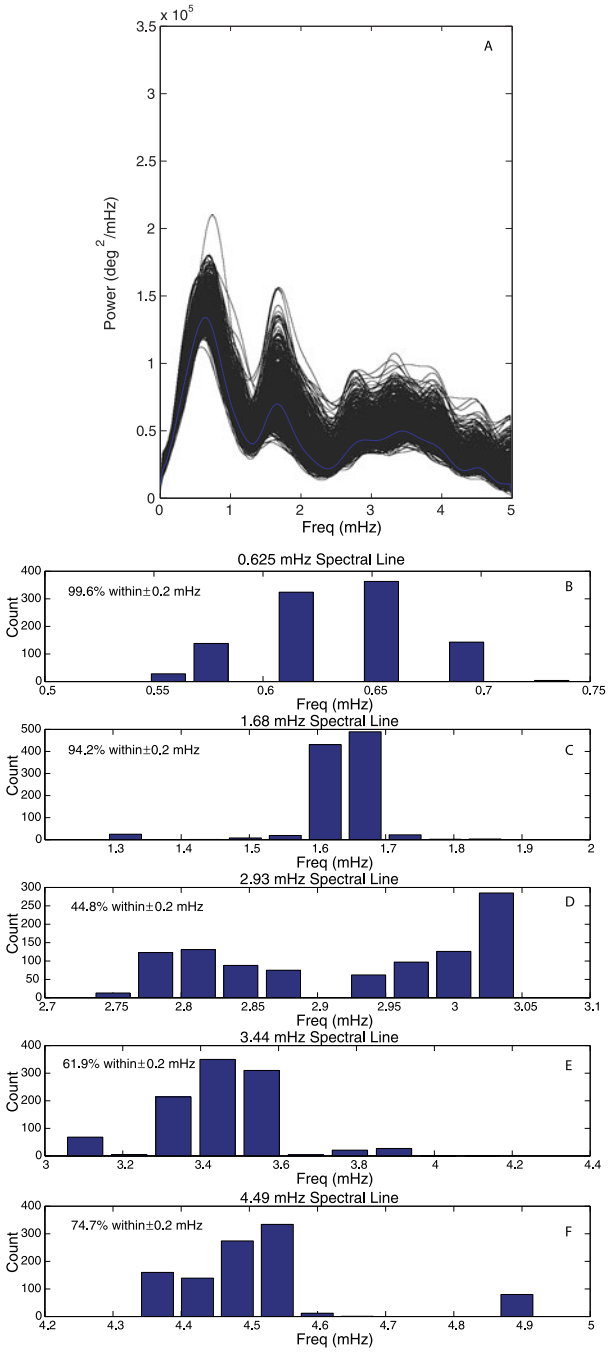

Figure 6 (Panel A) Monte Carlo simulated FRF spectra for 10 November 2009 (black). Spectrum from Figure 4 (right, 0.5 mHz highpass) is shown in blue; there are five possible spectral lines present. (Panels B – F) For each spectral range shown, the frequency of the local maximum is counted from the Monte Carlo simulation and plotted in a histogram.

this is the case in Figure 7 as well around 2.93 and 3.95 mHz. Only those spectral line(s) with 1 σ or more standard deviations above the mean are shown in Table 2.

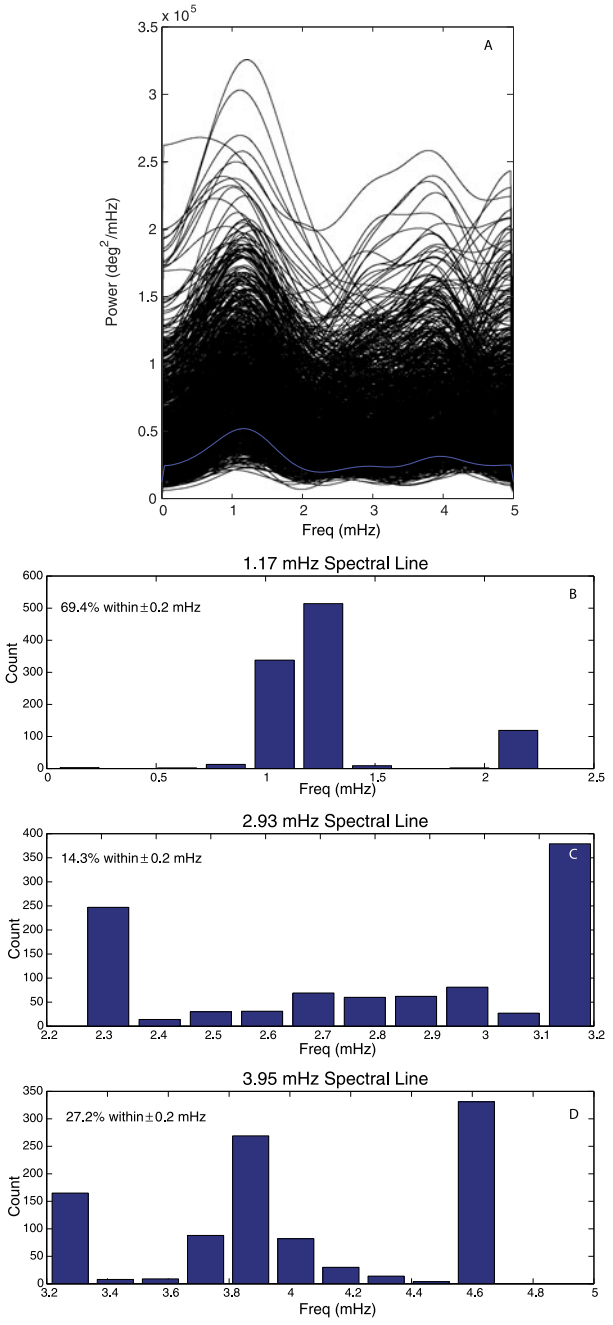

Figure 7 (Panel A) Monte Carlo simulated FRF spectra for 11 November 2009 (black). Spectrum from Figure 5 (right, linear) is shown in blue; there are three possible spectral lines present. (Panels B – D) For each spectral range shown, the frequency of the local maximum is counted from the Monte Carlo simulation and plotted in a histogram.

5. Results

Two trends are apparent in the data set summarized by Table 2: wave power decreases with increasing frequency and with increasing distance from the Sun. A falloff in power with

Table 2 Characteristics of the FRF spectral lines and ranges in offset distance during the observation time periods. Note: The spectral line in bold is reliable to two standard deviations (SDs), and the rest are reliable to one SD.

Date	Offset (Solar Radii)	Line frequency (mHz)	Reliability (%)	Power ($deg^2\,mHz^{-1}$)
10 November	1.55 – 1.85	**0.625**	**99.6**	**134.0**
		1.68	94.2	69.8
		4.49	74.7	22.5
11 November	3.11 – 3.22	1.17	69.4	51.9

increasing frequency in FRFs across the frequency range 0.5 to 5 mHz has been observed in all previous (turbulence) experiments. Similarly, investigations into the change in FRF spectral index (the change in spectral density power with frequency) with distance from the Sun all show a similar behavior (see, e.g., Andreev *et al.*, 1997a; Chashei *et al.*, 2000; Bird, 2007).

Waves with periods similar to those in Table 2 have been observed closer to the solar surface by the *Transition Region and Coronal Explorer* (TRACE) spacecraft. Van Doorsselaere, Birtill, and Evans (2009) described observations of closed coronal-loop fluctuations with frequencies of 1.12 mHz (similar to 11 November). Longer-wavelength fluctuations in coronal loops have been documented by De Moortel and Brady (2007) with frequencies ranging between 0.4 and 1 mHz, including 0.625 mHz. Finally, spectral lines around 4.49 mHz in frequency were discovered in FRF observations by Andreev *et al.* (1997a, 1997b).

6. Conclusions

The plasma of the solar corona is strongly influenced by the magnetic field. However, it is challenging to observe the magnetic field outside of active regions to investigate its role in transferring energy throughout the corona and solar wind. Only the phenomenon of Faraday rotation can make remote sensing observations of this "invisible" magnetic field. In the solar corona, Faraday rotation fluctuations are dominated by Alfvén waves. Occasionally these MHD waves will generate spectral lines in the general turbulent Faraday rotation fluctuation spectrum, allowing closer investigation into the corona's magnetic wave efflux energy (Jensen and Russell, 2009).

In November 2009, toward the end of the longest solar minimum in a century, the MESSENGER spacecraft was in superior conjunction, a geometry that allowed the measurement of the solar magnetic field using Faraday rotation. We show that on 10 November 2009 a reliable Faraday rotation fluctuation spectral line was observed at 0.6 mHz around a solar offset distance of 1.7 solar radii. Previous spectral lines have been observed between 4 and 8 mHz at offset distances around 5 to 10 solar radii. Alfvén waves of the same frequency as the MESSENGER spectral line have been observed traveling along coronal loops nearer to the solar surface.

The solar corona evolves both structurally and energetically as it expands. Faraday rotation fluctuation observations of the MHD waves present under varying solar activity, structure, and offset distances provide valuable information into the dynamics of the solar wind, the main driver of Earth's "space weather."

Acknowledgements The authors thank Andy Breen, Andy Buffington, John Clover, Richard Fallows, Bill Feldman, Carl Heiles, Ken'ichi Fujiki, P.K. Manoharan, Jean-Luc Margot, Ralph McNutt, Toney Minter,

Divya Oberoi, Karen O'Neil, Mark Perry, Christopher Russell, Sean Solomon, Munetoshi Tokumaru, the MESSENGER spacecraft team for coordinating the spacecraft's operations to perform this experiment, and NRAO's Green Bank Telescope team for facilitating the observations taken on the Earth. This research was supported by the MESSENGER Participating Scientist program and ACS Consulting, LLC.

References

Andreev, V.E., Efimov, A.I., Samoznaev, L.N., Chashei, I.V., Bird, M.K.: 1997a, Characteristics of coronal Alfvén waves deduced from HELIOS Faraday rotation measurements. *Solar Phys.* **176**, 387 – 402.

Andreev, V.E., Efimov, A.I., Samoznaev, L.N., Chashei, I.V., Bird, M.K.: 1997b, Properties of coronal Alfvén waves from polarized radio occultation experiments. *Adv. Space Res.* **20**, 65. doi:10.1016/S0273-1177(97)00482-1.

Armstrong, J.W., Coles, W.A.: 1972, Analysis of three-station interplanetary scintillation. *J. Geophys. Res.* **77**, 4602 – 4610. doi:10.1029/JA077i025p04602.

Belcher, J.W., Davis, L. Jr.: 1971, Large-amplitude Alfvén waves in the interplanetary medium, 2. *J. Geophys. Res.* **76**, 3534 – 3563. doi:10.1029/JA076i016p03534.

Bird, M.K.: 1982, Coronal investigations with occulted spacecraft signals. *Space Sci. Rev.* **33**, 99 – 126. doi:10.1007/BF00213250.

Bird, M.K.: 2007, Coronal Faraday rotation of occulted radio signals. *Astron. Astrophys. Trans.* **26**, 441 – 453. doi:10.1080/10556790701595236.

Bisi, M.M., Breen, A.R., Jackson, B.V., Fallows, R.A., Walsh, A.P., Mikić, Z., Riley, P., Owen, C.J., Gonzalez-Esparza, A., Aguilar-Rodriguez, E., Morgan, H., Jensen, E.A., Wood, A.G., Owens, M.J., Tokumaru, M., Manoharan, P.K., Chashei, I.V., Giunta, A.S., Linker, J.A., Shishov, V.I., Tyul'Bashev, S.A., Agalya, G., Glubokova, S.K., Hamilton, M.S., Fujiki, K., Hick, P.P., Clover, J.M., Pintér, B.: 2010, From the Sun to the Earth: the 13 May 2005 coronal mass ejection. *Solar Phys.* **265**, 49 – 127. doi:10.1007/s11207-010-9602-8.

Bisi, M.M., Fallows, R.A., Jensen, E.A., Breen, A.R., Xiong, M., Jackson, B.V.: 2011, Current and planned solar wind observations using the EISCAT and LOFAR radio-telescope systems. *AGU Fall Meeting Abstracts*, Abstract #SH31C-2020.

Chashei, I.V., Bird, M.K., Efimov, A.I., Andreev, V.E., Samoznaev, L.N.: 1999, Five-minute magnetic field fluctuations in the solar wind acceleration region. *Solar Phys.* **189**, 399 – 412.

Chashei, I.V., Samoznaev, L.N., Bird, M.K., Pätzold, M.: 2000, The spectrum of magnetic field irregularities in the solar corona and in interplanetary space. *Adv. Space Res.* **25**, 1973 – 1978. doi:10.1016/S0273-1177(99)00614-6.

De Moortel, I., Brady, C.S.: 2007, Observation of higher harmonic coronal loop oscillations. *Astrophys. J.* **664**, 1210 – 1213. doi:10.1086/518830.

Esser, R., Habbal, S.R., Withbroe, G.L., Leer, E.: 1986, A two-fluid solar wind model with Alfvén waves – parameter study and application to observations. *J. Geophys. Res.* **91**, 2950 – 2960. doi:10.1029/JA091iA03p02950.

Hewish, A., Scott, P.F., Wills, D.: 1964, Interplanetary scintillation of small diameter radio sources. *Nature* **203**, 1214 – 1217. doi:10.1038/2031214a0.

Hollweg, J.V.: 1986, Transition region, corona, and solar wind in coronal holes. *J. Geophys. Res.* **91**, 4111 – 4125. doi:10.1029/JA091iA04p04111.

Hollweg, J.V., Bird, M.K., Volland, H., Edenhofer, P., Stelzried, C.T., Seidel, B.L.: 1982, Possible evidence for coronal Alfvén waves. *J. Geophys. Res.* **87**, 1 – 8. doi:10.1029/JA087iA01p00001.

Jensen, E.A., Bisi, M.M., Breen, A.R., Heiles, C., Minter, T., Vilas, F.: 2012, Measurements of Faraday rotation through the solar corona during the 2009 solar minimum with the MESSENGER spacecraft. *Solar Phys.*, this issue.

Jensen, E.A., Russell, C.T.: 2009, Coronal magnetic field analysis with Faraday rotation observations of Alfvén waves. *Geophys. Res. Lett.* **36**, 5104. doi:10.1029/2008GL036257.

Sakurai, T., Spangler, S.R.: 1994, The study of coronal plasma structures and fluctuations with Faraday rotation measurements. *Astrophys. J.* **434**, 773 – 785. doi:10.1086/174780.

Salah, J.E., Lonsdale, C.J., Oberoi, D., Cappallo, R.J., Kasper, J.C.: 2005, Space weather capabilities of low frequency radio arrays. In: Fineschi, S., Viereck, R.A. (eds.) *Society of Photo-Optical Instrumentation Engineers (SPIE) Conference Series* **5901**, 124 – 134. doi:10.1117/12.613448.

van Doorsselaere, T., Birtill, D.C.C., Evans, G.R.: 2009, Detection of three periodicities in a single oscillating coronal loop. *Astron. Astrophys.* **508**, 1485 – 1491. doi:10.1051/0004-6361/200912753.

Welch, P.D.: 1967, The use of fast Fourier transform for the estimation of power spectra: a method based on time averaging over short, modified periodograms. *IEEE Trans. Audio Electroacoust.* **AU-15**, 70 – 73.